Electrocatalysis at Single Nanoparticles

Kleijn, S.E.F.

4

Influence of hydrazine-induced aggregation on the electrochemical detection of platinum nanoparticles

Abstract

To study the catalytic activity of single nanoparticles (NPs) electrochemically, we investigated the applicability of a novel method for nanoparticle detection as a means to immobilize individual NPs. This method consists of analyzing the current steps that can be measured at an ultramicroelectrode (UME) when a colloid of NPs is injected into an electrolyte containing an electroactive species, that is turned over at the NP but not the UME surface. We have measured these current steps for the hydrazine oxidation at Pt NPs landing on a lithographically fabricated Au UME, showing a mean step size comparable to theory and prior measurements. We found a reduced landing frequency with respect to values reported in the literature and those predicted from theory, while the current step distribution showed a long tail of large current steps. This could be explained by the particle aggregation, which would lower the effective NP concentration and therefore lower the landing frequency and would result in higher current steps when aggregates reach the electrode. Cyclic voltammetry (CV) measurements of the Pt-modified Au UME showed a signal characteristic of the presence of Pt, while electron microscopy revealed aggregated NPs, after landings were performed in the presence of hydrazine or hydrogen gas. Conversely, no aggregates were found after particles were injected in absence of such reducing agents, while CV still suggested the presence of Pt, indicating individual particles. The finding, that landing nanopar-

ticles in the presence of hydrazine yields NP aggregates on the surface, means that this particular method is currently not suited for the preparation of individually immobilized particles to facilitate catalysis studies at individual nanoparticles.

4.1 Introduction

Metal nanoparticles (NPs) are employed in a wide variety of scientific subjects and technical applications.[1, 2] In applications such as catalysis such particles present, above all, a large surface-to-weight ratio that is instrumental to cost abatement when using expensive metals. Moreover, the exact shape and size of a metal particle can influence its characteristics. For instance, surface plasmons of gold particles change in energy with the particle dimension,[3] and in heterogeneous catalysis there is an ongoing debate about the dependence of catalytic activity on particle size and shape.[4–6] In catalysis, it is assumed that for every reaction there exists an optimal particle size that is presently determined through analysis of large particle populations in macroscopic screening experiments.[7, 8] The results of these measurements are compared to the particle size distribution that is determined through e.g. TEM imaging. The ability to measure the activity of individual particles would circumvent the statistics involved in ensemble studies and point out exactly which part of the size distribution is most active. In other areas of catalysis, great advances have been made to study the activity of individual catalyst particles. The interactions inside individual zeolite particles have been elucidated in heterogeneous catalysis,[9] while the biocatalytic properties of individual enzymes have also been revealed using confocal microscopy.[10] Electrocatalytic measurements are very promising in this respect, because very small electrochemical currents can be detected. Measurements on individual catalyst particles in electrochemistry have been performed on a single Pt nanoparticle electrodeposited on the tip of thin carbon fibre UME,[11, 12] on nanoparticles attached to the side walls of carbon nanotubes,[13] and on an extremely small number of enzymes immobilized on a Au UME.[14]These measurements open up a path to the study of single particles with size distributions found in applied catalysis.

Recently, a new electrochemical method has been introduced to monitor individual nanoparticles by detecting their arrival at the conducting surface of an ultramicroelectrode (UME). The idea of the method is illustrated schematically in figure 4.1. The UME is placed in a solution containing some electroactive species as well as catalytic nanoparticles (NP), and held at a potential at which the electrochemical reaction does not occur at the UME surface, but does occur at the surface of the nanoparticles if they

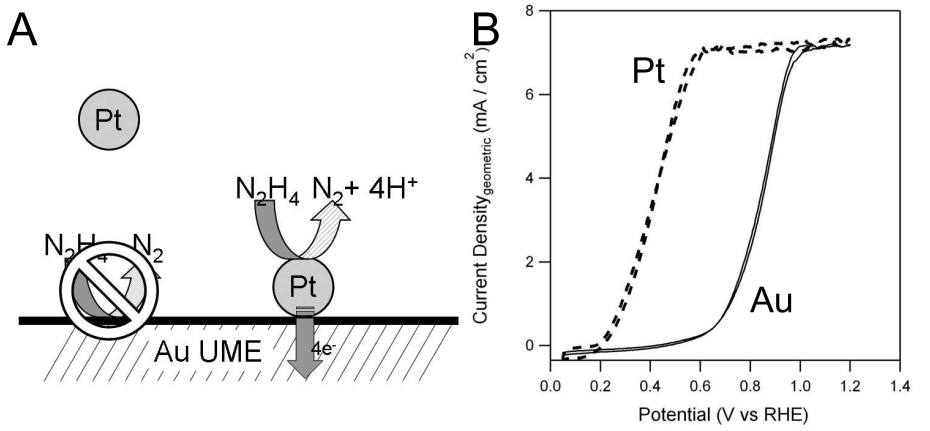

Figure 4.1: (A) The principle of nanoparticle detection mediated by the oxidation of hydrazine is schematically displayed: At a given potential, hydrazine will not be oxidized at a Au surface, while a Pt particle attached to gold will catalyze this reaction. (B), Current-Voltage plots of the hydrazine oxidation measured at Pt and Au rotating disk electrodes, depicting the difference in the onset potential of hydrazine oxidation on Pt (dashed) and Au (full) electrodes. These measurements were performed at 700 RPM and 50 mV $s^{-}1$in a 50 mM phosphate buffer of pH 8, containing 5 mM hydrazine.

make contact with the UME electrode surface at random. An appropriate combination of electrode material, nanoparticle material and electrochemical reaction ensures that the UME surface gives no electrochemical signal, so that all the electrochemical activity must come from colliding nanoparticles. After being introduced to the system, the nanoparticles will randomly approach the electrode surface and so far two types of UME-NP interactions have been observed: a current step[15–18], and a current spike that decays to background level.[19–27] A staircase response is indicative of a cumulative immobilization of active particles on the UME surface. This type of response was observed for the first time in the Bard group, upon adding a dilute solution of Pt NPs to a neutral electrolyte containing a low concentration of hydrazine (N_2H_4) and a Au UME held at a potential where hydrazine is oxidized at Pt but not at Au. [16]

A spike-type response, on the other hand, signifies a fleeting interaction, either because the particle is oxidized completely, or because it briefly performs a reaction before departing from the surface. In the Compton group, current spikes were measured for the direct oxidation of Ag NPs at a carbon UME.[21] In these spikes a charge was passed corresponding to the ionization of nanoparticles when the electrode was held at a potential above the oxidation of the silver metal. In another measurement,[19]

a Pt UME was passivated by oxidizing its surface at a high potential, and subsequently iridium oxide particles where added that catalyze the oxygen evolution reaction. Current spikes were observed suggesting that the nanoparticles were only briefly contacting the surface.

The frequency at which these landings occur has been reported to depend linearly on NP concentration with average molar collision frequencies of $1.5x10^4$ - $2.5x10^4$ $s^{-1}pM^{-1}cm^{-2}$ [16] and $3.9x10^4$ $s^{-1}pM^{-1}cm^{-2}$.[21]

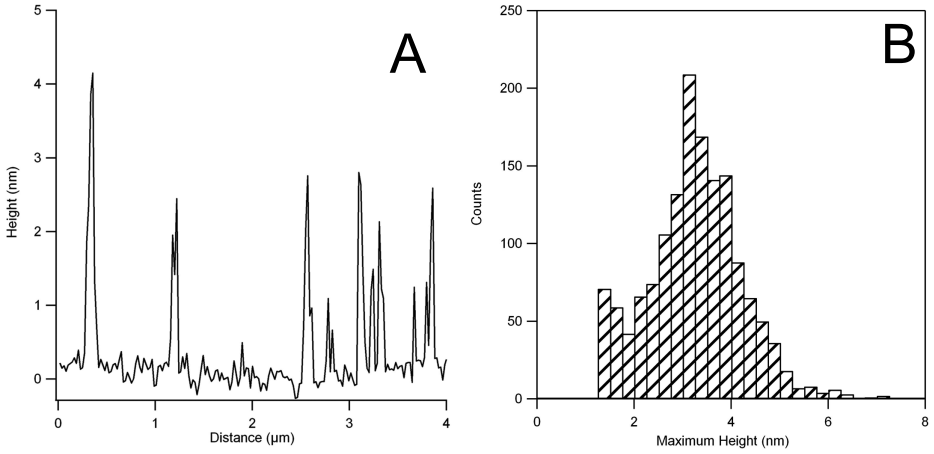

Figure 4.2: A) Linescan of a typical AFM measurement of Pt nanoparticles freeze-dried on silicon. B) Pt NP- height distribution measured using AFM, revealing the mean particle size.

This method for detecting nanoparticles could very well be applied to the study of the catalytic activity of individual particles. In order to realize this, it is necessary to verify that substrates, after showing a specific number of 'landing events' during electrochemical detection, have an equivalent number of homogeneously distributed nanoparticles stuck to the electrode surface. If so, one could aim to control the number of landings so as to study the electrocatalysis of a controlled number of nanoparticles.

Therefore, in this chapter we show ex-situ measurements after landing experiments in order to ascertain what is present on the metal surface. We report the detection of Pt nanoparticles using a Au ultramicroelectrode (UME); subsequently we show electron micrographs and cyclic voltammograms to characterize the composition of the electrode surface before and after measuring landing events. These measurements suggest that a landing event detected by hydrazine oxidation does not necessarily correspond to the arrival of an individual nanoparticle. In fact, we present evidence that

the presence of a strong reducing agent, such as hydrazine and hydrogen, may induce aggregation of ligand-capped nanoparticles in solution.

4.2 Experimental

4.2.1 Materials

Sulfuric acid (UltraPur), sodium di-hydrogen phosphate and di-sodium hydrogen phosphate (both, pro analysi) salts and tri-sodium citrate dihydrate (pro analysi) were purchased from Merck, hydrazine hydrate (98%), chloroplatinic acid hydrate (99.9%) was purchased from Sigma-Aldrich. Sodium Borohydride (98+%) was purchased from Acros Chemicals. Before starting a measurement, argon gas with a purity grade of 6.0 was bubbled through the electrolyte (prepared using MilliQ water of 18 M cm resistivity) to remove the majority of atmospheric oxygen. In measurements using hydrogen gas, hydrogen of 5.0 purity grade (BIP Grade, AirProducts) was bubbled through the electrolyte solution.

4.2.2 Lithographical fabrication of microelectrodes

The electrodes used in this experiment were lithographically produced Au UMEs on a chip, the fabrication of which has been detailed in Appendix A. In summary, we pattern electrodes and their electronic leads in a bi-stack of PMGI and PMMA using an electron beam pattern generator at 100 kV (EBPG5000+, Vistec).The pattern is filled with 2 nm of an adhesive Ti layer and a Au layer of 70 nm by electron beam evaporation. To protect all but a controlled electrode surface area from the electrolyte, we first cover the entire chip with a thick (400nm) SiN passivation film by Plasma Enhanced Vapor Deposition. In a subsequent electron beam lithography step, the 100 x 50 μm^2 area containing the electrodes is de-protected by Reactive Ion Etching of the SiN in a plasma of CHF_3 and O_2. This last step exposes eight nanoelectrodes (varying in size from 50x500 nm^2 to 1000x500 nm^2) and one microelectrode of 100 x 20 μm^2. The successful outcome of the microchip fabrication was verified by Scanning Electron Microscopy (SEM, FEI Nova 200 NanoSEM) and cyclic voltammetry.

Electrolyte is provided in a flow-cell setup from a 200 mL volume containing the electrolyte and a reference electrode. By applying slight argon overpressure to the electrolyte, it flows through 30 cm of Halar or Teflon tubing into a PEEK cell that is firmly depressed onto the chip with a Viton O-ring. During measurements, the electrolyte is flowing (typical flow-rate ~1 ml/min) for the first two minutes after injection, to

ensure that the nanoparticle concentration near the chip is equal to that in the solution, afterwards the argon pressure is released to stagnate the electrolyte flow.

4.2.3 Electrochemical Measurements

The current flowing through the electrode is measured using a Stanford SR570 I-V amplifier, the output of which is read by the same analog-to-digital converter (NI USB-6251) that is used to apply a potential between the UME and a reference electrode that also functions as the counter electrode. In most experiments the reference electrode was a mercury-mercurous sulfate electrode (MSE; Radiometer Analytical XR230), while in some cases a Pt flag (~4.5 cm^2) was used as a reference electrode. Data collection is performed using LabView. The measurement was performed inside a Faraday cage to minimize interference to the signal. Landing measurements were performed in a phosphate buffer at pH 8, with a concentration of 10 mM. These conditions are close to those reported in earlier, similar experiments[16] and were chosen because extreme pH values and high buffer salt concentrations tend to aggregate nanoparticles in solution. When going through a range of buffer concentrations (from 1 mM to 100 mM phosphate) and pH values (pH 6 and pH 8), we have not found a significant change in experimental behaviour and therefore measurements at only one value (10 mM) are shown herein.

For comparison with the literature, measurements were also performed using a commercial Au UME with a diameter of 25 µm (CHI106, CH Instruments), in a glass cell with 100 mL of electrolyte. Measurements were performed using the same instrumentation as mentioned above, in a two-electrode setup with a commercial MSE reference electrode as the second electrode.

Rotating Disk Electrode (RDE) measurements were performed using a Pine Instruments (AFMSRXE) system, employing 5 mm Au and Pt disk electrodes supplied by Pine Instruments, and coiled Au and Pt wires respectively as counter electrodes whilst using the MSE as a reference.

4.2.4 Nanoparticle Synthesis

Nanoparticles were synthesized according to a recipe from the literature:[16, 28] to a stirred mixture of H_2PtCl_6 and Na_3Citrate, $NaBH_4$ was added dropwise. We used the following molar concentrations: 1 mmol :1 mmol :10mmol (Pt:Citrate:Borohydride) in 20 mL of water. The resulting colloid does not show precipitation within several months.

The NP concentration was evaluated with AFM,[29] by freeze-drying a known volume of Pt colloid unto a known surface area of Si wafer. AFM measurements were performed on a Veeco/Bruker Multimode AFM microscope with a Nanoscope IIIa controller using Olympus AC 160TS Micro Cantilevers (tip radius $<$10nm). Data analysis on the images was performed using the WSxM software[30] to flatten the images (i.e. remove baseline contributions) and count the amount of particles and their height. An example of one of the linescans that constitute an AFM image is shown in Figure 4.2A. The 2D density of particles obtained in this way was then calculated back to the initial concentration to yield 1.4$\pm$0.5 µM, which is a factor 7.1 $\pm$ 2.6 x10^2 lower than the initial atomic concentration and therefore corresponds to a nanoparticle diameter between 2.6 and 3.3 nm.[31] To appreciate this value we may compare it with the particle height distribution determined by AFM which has a mean of 3.3$\pm$1.0 nm, shown in Figure 4.2B. In addition to this, particle size measurements were also performed using XRD on a Philips PAnalytical X'Pert system. The Scherrer formula[32] was used to estimate the crystallite size of the Pt NPs, resulting in a value of 3.8 nm for the average particle size, both for a freshly prepared solution and an aged solution. It should be noted that these sizes agree closely to those reported in the recipe that we have followed.[16, 28]

4.3 Results

In order to detect the landing events of the platinum nanoparticles on the gold electrode, we choose an electrochemical reaction that, at the selected potential, occurs only on the surface of the Pt nanoparticles and not at the gold electrode, in this case hydrazine oxidation. The difference in reactivity between Pt and Au can be appreciated from the different onset potentials for the oxidation of hydrazine in the CVs displayed in figure 4.1B. This reaction is catalyzed by platinum at potentials above 0.2 V vs. RHE,[33, 34] and a current response is expected when a Pt NP contacts the gold electrode if the gold electrode is polarized at a value higher than 0.2 V vs. RHE. In the landing measurements to be described below we have chosen values of 0.35, 0.45 and 0.55 V vs. RHE, where the background current is low because the onset of the hydrazine oxidation on the Au UME was found in our setup to start at 0.6 vs RHE. These values are comparable to those reported in the literature.[16, 35, 36]

Figure 4.3 shows a current-time measurement after adding 200 µL of citrate-capped Pt NPs (corresponding to 1.4$\pm$0.5 nmol/liter) to a solution of 10 mM hydrazine, and we observe changes in the current (in steps) presumably caused by the Pt nanoparticles

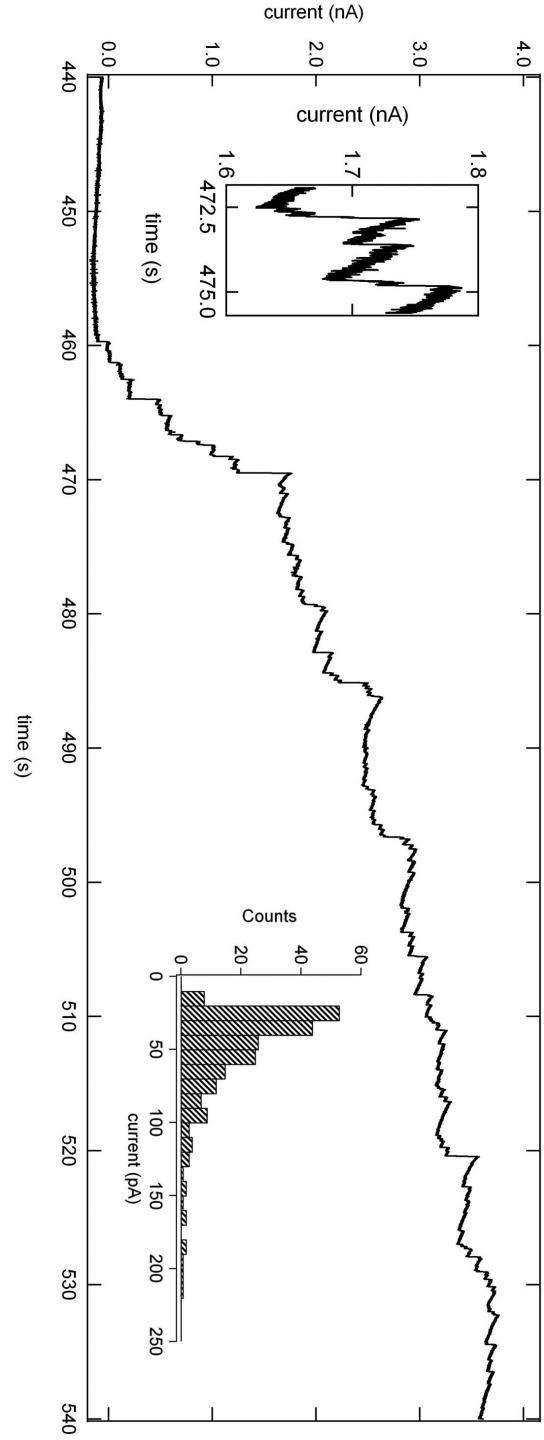

Figure 4.3: Discrete current increments caused by the oxidation of 10mM hydrazine at Pt NPs impacting onto the surface of a 2000 μm^2 Au UME, held at 0.35 V vs RHE, in 10 mM phosphate buffer of pH = 8. Inset on the right is the histogram of the step height distribution. Inset on the left is a magnification of some current steps.

landing on the surface of the gold electrode. After the initial step a slow decrease in current is observed. The time-constant for this decrease does not agree with those for capacitive discharging or Cottrell-type mass-transport effects. We therefore attribute this current decay to deactivation of the nanoparticles, presumably as a result of contamination, as has been suggested previsouly. [16] Before landing of the nanoparticles, the current is stable and slightly cathodic, which can be ascribed to the reduction of a trace of oxygen. The cascades of collisions take place with an average landing frequency of ~2 landings s^{-1}. This landing frequency is lower than the expected value extrapolated from the literature,[15, 16, 21] even though in our experiments the nanoparticle concentration and the area of the microelectrode used are both higher than values reported in other experiments. It should be noted that no difference in the landing frequency was found between conditions of flowing or stagnant electrolyte. When we perform the same measurement using a glass sealed Au UME, we also obtain a lower landing frequency than expected (~0.02 landings s^{-1} at equal concentration, while the electrode surface area is four times smaller than the surface area of the lithographically fabricated UME), as can be seen in Figure 2 of Appendix B. The landing frequency reported by Bard et al. [16] for the hydrazine-mediated detection of Pt NPs, is 0.01 $s^{-1}pM^{-1}$, or 10 landings per second extrapolated to our particle concentration, on an electrode with a surface area that is twenty-five times smaller than the one employed in our study.

The nanoparticle landing frequency may be estimated according to Fick's law, assuming diffusion-limited steady-state conditions:[16, 37]

$$J = \kappa\chi D_{NP} C_{NP} \tag{4.1}$$

where κ is a sticking coefficient ($0 < \kappa < 1$), χ is geometry factor (for a disk, $\chi = 4/\pi a$, with a the UME radius), D_{NP} the nanoparticle diffusion coefficient and C_{NP} their concentration in solution. In our experiment we can accurately determine the surface area of the UME, and the diffusion coefficient is a constant, that can be calculated from the Stokes-Einstein equation

$$D = \frac{k_b T}{6\pi\eta r} \tag{4.2}$$

depending only on the particle radius r and the solution viscosity η as variables. The viscosity for water is a known constant, and the particle radius as well, albeit with a some uncertainty. However, this uncertainty does not explain the observed deviation in the landing frequency. The geometry factor χ of our system is quite complicated

and requires numerical calculations to be determined exactly, but it is constant. We have previously simulated the diffusion of species to similar UMEs[38] and the resulting flux is comparable to the theoretical flux to similar sized, disk-shaped electrodes. Therefore we do not expect the particular geometry of our system to account for a large change in the landing frequency. The sticking coefficient κ, a factor indicative of the probability that a particle attaches to the surface upon colliding with it, was introduced by Bard et al.[18] to accommodate for a deviation between the experimentally observed and theoretically predicted landing frequency (when κ = 1). We however have no adequate means to estimate the value for κ. Finally, the nanoparticle concentration is calculated from the estimated nanoparticle size. This value can however change greatly if the particles aggregate in solution, prior to landing. Large particle clusters can form during aggregation in solution, lowering significantly the concentration of non-aggregated nanoparticles in solution. Further results below indicate that aggregation indeed seems to occur during our measurements.

The inset on the left in Figure 4.3 shows a detail of the current step, where the initial spike amplitude was used as the current step height value in order to establish the distribution of current step heights from the landing events (shown on the right in Figure 4.3). A broad distribution of peak heights is observed, ranging between 20–200 pA, while the modal current values are between 20 and 50pA. The mean current step height will include the the higher values in the tail of the distribution and is therefore higher. Theoretically, the current step amplitude should be related to the radius of the incoming nanoparticle, as well as to the concentration of hydrazine (see equation 3 below), and therefore this amplitude distribution in one experiment should reflect the nanoparticle size distribution. Size measurements on colloidally synthesized nanoparticles generally show a normal distribution of the particle diameter and we have observed the same in our AFM measurements, but the peak height distribution we measure shows a much broader tailing distribution, that should however still be linked to the size distribution of the colliding nanoparticles.

The observed distribution in Figure 4.3 can be fitted with a convolution of Gaussian curves, as has been performed for other nanoparticle landing experiments.[27] In their experiments, Rees et al. showed that the data presented several normal distributions with a mean value related to a function of a multiple of the initial NP radius, suggesting nanoparticle aggregation.

Returning to the idea that the current steps correspond to the landing of an individual nanoparticle, the nanoparticle radius can be related to the measured current step, if we assume that the particle oxidizes hydrazine at the diffusion limited current,

according to the following equation for the theoretical diffusion limited current at spherical particles suspended on a plane: [16]

$$I = 4\pi(ln2)nFD_{HZ}C_{HZ}r_{NP} \tag{4.3}$$

where n is the electron transfer (4 electrons in this reaction), $F$is Faraday's constant, C_{HZ} is the concentration of hydrazine (10 µmol cm^{-3}) and r_{NP} is the nanoparticle radius. A wide range of diffusion coefficients for hydrazine (D_{HZ}) has been reported in the literature, ranging from 3.2 x 10^{-6} cm^2 s^{-1}[39] to 2.37 x 10^{-5} cm s^{-1}.[40] Moreover, values for D_{HZ} can be derived from publications in which they are not mentioned explicitly, yielding 1x10^{-6} cm^2 s^{-1},[36] 2x10^6 cm^2 s^{-1}, [33] and 1x10^{-5} cm^2 s^{-1},[35] whereas from the UME measurements reported by Bard et al.[16] a diffusion coefficient of 6.3 x 10^{-6} cm^2 s^{-1} is estimated. From the diffusion-limited current value in figure 4.1B, using the Levich equation, we obtain a diffusion coefficient of 6.4 x 10^{-6} cm^2 s^{-1}. This variance in D_{HZ} suggests that the diffusion limited current for hydrazine is very much dependent on measurement conditions, as otherwise a more unambiguous number would have arisen. Choosing the value measured in the RDE experiment we expect a current step of ca. 36 $\pm$11 pA for a particle of 3.3$\pm$1.0 nm diameter in a solution with 10 mM of hydrazine. We emphasize here that equation 3 applies specifically to spheres on infinite planes. If a NP would land on another NP already sticking to the surface, the flux of electrocatalytic substrate to the ensemble would be smaller and a lower current step would be expected. This should hold especially for the case of a particle impacting on an aggregate of particles at the surface.

Particle aggregates should yield a higher value than the current for a single particle, however, this factor is influenced heavily by the geometry and density of the aggregate since a catalytic reaction must be performed at the constituent surface of the NP aggregate. Nevertheless, we suppose that the very high landing currents (of around 200 pA) should be ascribed to aggregated particles sticking to the surface.

Figure 4.4 shows the current step distributions at three electrode potentials, i.e. 0.35, 0.45, 0.55 V vs RHE. For all potentials, most current steps are reasonably close to the theoretical estimate of 36 pA, which appears to confirm the model suggested by Eq.3 for the selected diffusion coefficient. The lack of increase in current at higher potentials suggests that the reaction is in a diffusion-limited regime. This does not correspond well to the CV for a Pt RDE, shown in figure 4.1B, and implies that at a Pt nanoparticle the current-voltage characteristics are not the same as at a macroscopic disk. The current steps are also very similar to those observed in the literature, [16] though, as mentioned, our landing frequency is always considerably lower.

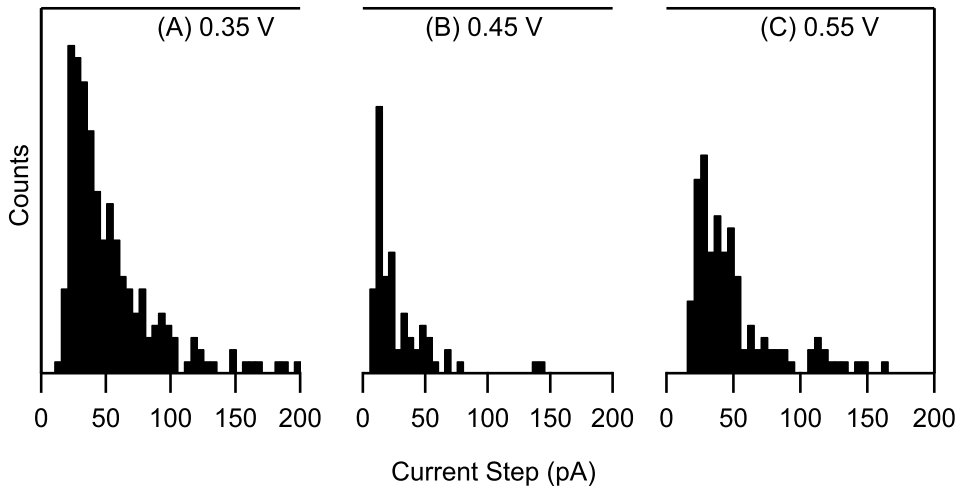

Figure 4.4: Current step height distributions measured at three UME potentials.

In order to verify the presence of the Pt NPs on the Au UME, cyclic voltammograms of the Au UME are measured in sulfuric acid before and after the landing experiment. Figure 4.5 shows the two CVs, with the dashed line corresponding to the gold electrode before the addition of Pt NPs and the black curve to the gold electrode after landing Pt NPs. The dotted curve agrees well with the blank CV of gold in sulfuric acid.[41] In the CV measured after landing Pt NPs, by comparison with the clean Au CV, we conclude that most of the underlying gold is still in contact with the solution, judging from the charge passed during surface oxidation and reduction between 1.0 and 1.6 V. However, the presence of Pt on the Au UME is also evidenced. A major difference in hydrogen evolution current is seen at 0 V, a reaction for which platinum is a far more active catalyst than gold. Also features indicative of the adsorption and desorption of underpotential deposited hydrogen on the Pt surface are observable between 0.1 and 0.3 V, while the small anodic and cathodic features near 0.7 and 0.6 V, resp. correspond to the surface oxide formation and subsequent reductive stripping on a Pt electrode.

After having deposited the nanoparticles on the Au UME, Scanning Electron Microscopy (SEM) is used to inspect the electrode surface, and Figure 4.5B shows a micrograph overview of the UME surface. Rather than single particles, we observe large aggregates of nanoparticles (in bright white) uniformly dispersed over the sur-

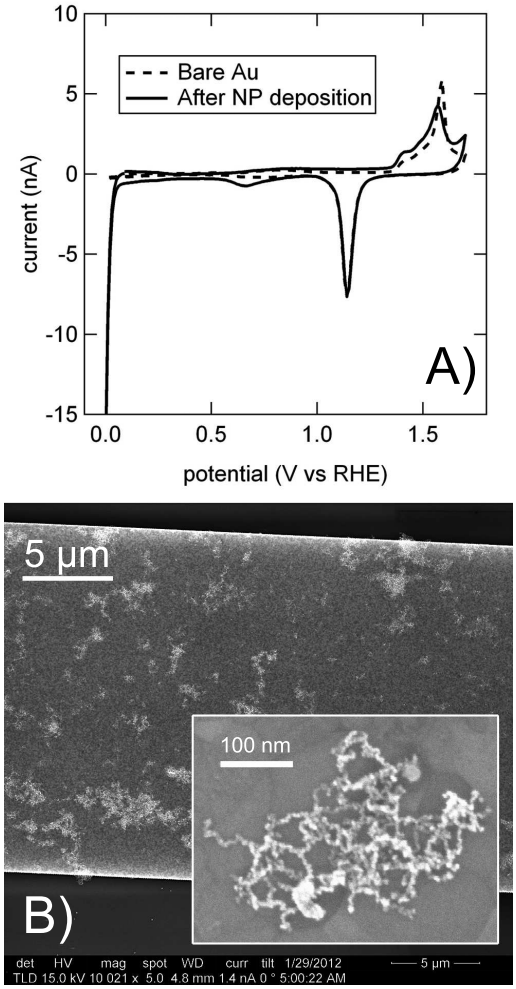

Figure 4.5: (A) Cyclic voltammograms of the gold UME in 0.1M H_2SO_4 before (dotted line) and after (black line) landing events using hydrazine oxidation as a detection reaction at 0.35 V vs. RHE. In the gold CV after landing events (black line) electrochemical signals due to the presence of platinum can be clearly observed: Pt surface oxidation and reduction between 0.6 and 0.85 V, and hydrogen evolution around 0 V. (B) SEM image of the same Au UME after landing Pt NPs on the electrode using hydrazine oxidation as electrochemical detection reaction, with an inset magnification showing a Pt NP aggregate.

face of the gold electrode. A magnification of Figure 4.5B shows in more detail the chain-like two-dimensional structure of the NP aggregate, which suggests diffusion

limited aggregation of the nanoparticles as will be discussed below. The question now arises whether these aggregates form in solution, or upon landing on the Au electrode.

To test the influence of the various parameters in our system on the formation of nanoparticle aggregates, we perform the NP landing experiment at the same potential and for the same length of time, but in absence of hydrazine. In the absence of electrocatalytic substrate, discrete current events were not detected.

To show the presence of Pt on the Au UME, cyclic voltammetry was performed before and after addition of Pt NPs. The dashed curve in Figure 4.6 corresponds to the surface of the gold electrode before the experiment, while the black curve is for the same surface after addition of nanoparticles. The Au UME has been clearly modified by the presence of Pt on its surface. Again the hydrogen evolution indicative of the presence of platinum is observed and a cathodic current wave corresponding to the oxygen reduction reaction on platinum is observed negative of ~0.6 V (as we were unable to remove this small trace of oxygen in our experiment). SEM measurements performed after the Au UME had been in contact with the nanoparticle solution show no visible aggregates on the electrode surface, as shown in Figure 4.6B and the inset magnification. We do not expect to be able to see individual particles as their diameter approaches the resolution of the scanning electron microscope. Therefore, we conclude that in the absence of hydrazine in this experiment, Pt NPs still land on the Au UME but they do not form aggregates. This experiment strongly suggests that hydrazine in fact causes the aggregation of nanoparticles in solution.

As we found that hydrazine favors the formation of aggregates of nanoparticles we have attempted to use another reducing agent that oxidizes selectively on Pt surfaces to detect landings in chronoamperometry. To this purpose, we saturated the electrolyte solution (10 mM phosphate buffer at pH 8) with hydrogen gas that would be oxidized on Pt but not on Au and repeated the experiment under the same conditions. However, we were unable to detect discrete landing events in the presence of hydrogen gas, but rather a continuous increase in anodic current, as shown in Figure 3 of Appendix B.

In Figure 4.7A three voltammograms are displayed, measured in sulfuric acid before and after addition of NPs in presence of hydrogen gas. We compare the oxidation of hydrogen on Pt NPs that were landed in presence of hydrazine (dashed) and in the presence of hydrogen (solid). The clean Au surface hardly shows any anodic current for the oxidation of hydrogen gas, while this is clearly amplified after landing Pt NPs onto the surface.

Figure 4.7B is a SEM image taken after measurements with dissolved hydrogen gas as electrocatalytic substrate. Aggregates of Pt NPs are observed, but in compar-

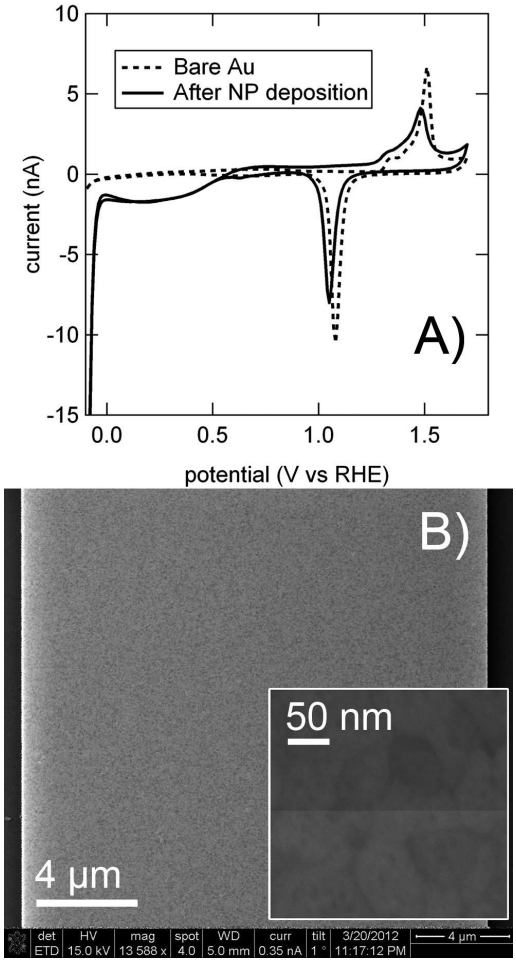

Figure 4.6: (A) Cyclic voltammetry of the gold before (dotted line) and after (black line) adding Pt nanoparticles in absence of hydrazine (in this measurement a Pt flag was used as a reference and counter electrode). In the gold CV after landing events (black line) electrochemical signals due to the presence of platinum can be clearly observed: Pt catalyzed hydrogen evolution around 0 V and an amplified oxygen reduction current below 0.6 V vs RHE. (B) SEM image after landing of Pt NPs on the Au electrode in the absence of hydrazine. No aggregates of Pt nanoparticles can be observed on the electrode surface.

ison with Figure 4.6B, a much smaller amount of aggregates exists on the electrode surface. This indicates that fewer particles are aggregated when using hydrogen gas to detect particles.

While hydrogen gas also acts as a reducing agent, and would also appear to facilitate the aggregation of NPs, much fewer aggregates are found after detecting landing events with hydrogen gas than in a comparable experiment using hydrazine. However, considering we use 1 bar of hydrogen gas to saturate the solution, the hydrogen concentration will be approximately 1 mM, which is an order of magnitude lower than the hydrazine concentration used in the other landing experiments. Combined with the question of the current step amplitude, we have therefore also studied nanoparticle landings with varying hydrazine concentration.

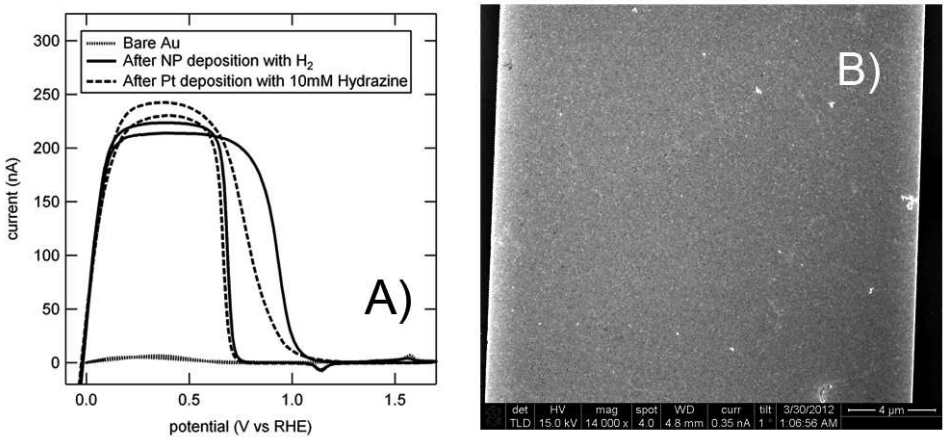

Figure 4.7: (A). Cyclic Voltammetry for the Au UME before (dotted line) and after Pt NP landing in presence of H_2 (solid line) or hydrazine (dashed line). The solution is 0.1 M H_2SO_4 saturated with H_2. (B) SEM image of the Au UME after injecting Pt NPs in the presence of H_2.

4.3.1 Influence of Hydrazine Concentration

The results of three Pt NP landing measurements performed at 0.1 mM, 1 mM and 50 mM of hydrazine are shown in Figure 4.8 and the results of 10 experiments are summarized in table 4.1. Chronoamperometric data of these experiments are shown in Figure 4 of Appendix B. Specifically, in table 4.1 the modal and mean current step heights are reported; the former should reflect the average individual particle size while the latter indicates the influence of higher current steps on the average, i.e. the amount of aggregates landing. Additionally, for clarity, the current step expected from theory for the landing of a Pt nanoparticle 3.3 nm in diameter is provided in the table as well.

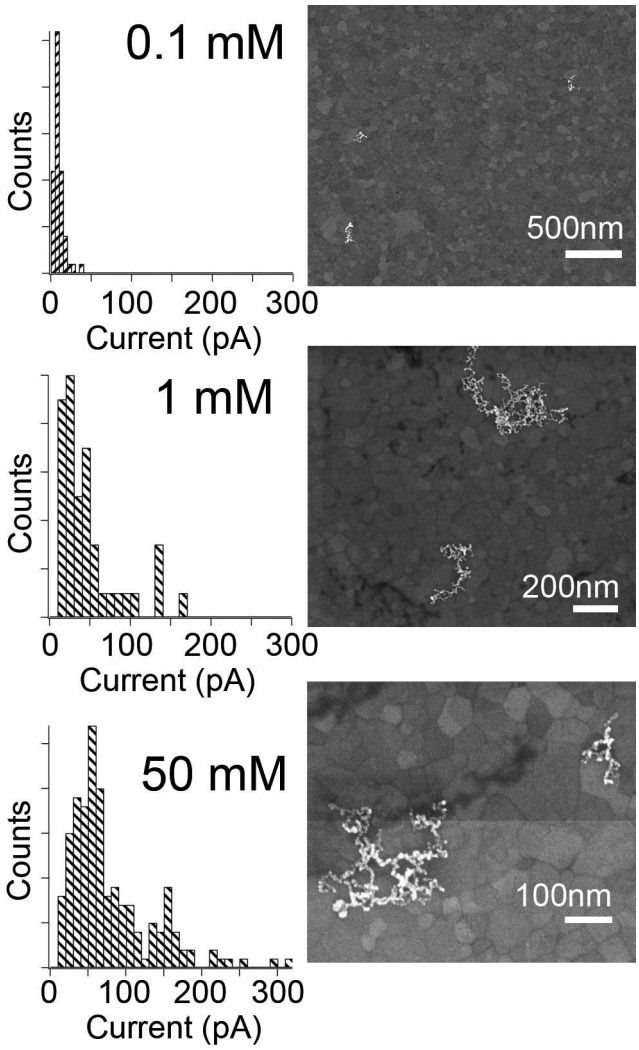

Figure 4.8: Histogram of the step height distribution, for various hydrazine concentrations, measurements were made at 0.35 V vs RHE. An increase in the mean current step height is observed with increasing hydrazine concentration.

These results do not display an obvious linear correspondence between the modes of the current step size distributions, the landing frequency, and the hydrazine concentration. Moreover, we did not find a clear trend in the relation between the mode and mean of the current step height distribution, suggesting that the degree of aggregation is not readily reproduced. Typically, we find that under seemingly identical conditions,

both the current step height and the landing frequency can vary widely. It is expected that the current steps would increase linearly with the hydrazine concentration, following equation 3 with values shown in the table. Although the results in Table 4.1 may suggest an increase in current step height with hydrazine concentration, the spread in the data is significant. When comparing the modes of the current step distribution to the expected value, the experimental values are always rather low, except in the case of very low hydrazine concentrations, when higher currents are measured. In the lower hydrazine concentration regimes, we may only detect the arrival of aggregates due to resolution limits, since landing events of individual particles would result in a neigh imperceptible current step on the picoampere level. Nevertheless, for the higher hydrazine concentrations currents remain lower than expected, which could be due to poisoning of the particle surface. Bard et al. [16] have reported a linear dependence of the peak current on the hydrazine concentration, but their reported experiments included only three data points over a limited hydrazine concentration (10-15 mM).

In all experiments, the SEM images show aggregated particles on the electrode surface after detecting the landings. Comparing the two extremes, after landing particles in 50 mM hydrazine there appear to be more aggregates on the surface of the electrode than in the case of 0.1 mM hydrazine. Noteably, there are more large aggregates present after landing particles with a higher hydrazine concentration. To ascertain the real difference in aggregate size, however, a detailed microscopy study has yet to be performed. Increasing aggregate size would suggest a decreasing landing frequency, but this is not evident from the data in table 4.1.

Hydrazine Concentration	Modal Current Step Height	Mean Current Step Height	Landing Frequency	Expected Current Step
0.1 mM	6 pA	9 pA	0.06 Hz	0.357 pA
1 mM	23 pA	44 pA	0.06 Hz	3.57 pA
5 mM	15 pA	25 pA	0.06 Hz	17.9 pA
10 mM	25 pA	58 pA	2 Hz	35.7 pA
10 mM	12 pA	27 pA	0.46 Hz	35.7 pA
10 mM	15 pA	59 pA	0.17 Hz	35.7 pA
10 mM	18 pA	25 pA	0.25 Hz	35.7 pA
20 mM	25 pA	30 pA	0.02 Hz	71.5 pA
20 mM	35 pA	82 pA	0.05 Hz	71.5 pA
50 mM	55 pA	86 pA	0.2 Hz	179 pA

Table 4.1: Observed landing frequencies and means of the current step height distributions for various concentration of hydrazine (corresponding current-time plots are shown in Appendix B).

To evaluate the influence of the surface potential of the electrode upon the formation of aggregates, we performed the experiment in the same conditions, in absence and presence of hydrazine, at various potentials. Potentials selected were the hydrogen evolution potential, the open-circuit potential and large overpotentials where hydrazine would oxidize on Au. In all these cases we could not reproducibly measure landing events. Here we have found systematically that only when hydrazine was present in the system, nanoparticle aggregates were found after a landing experiment.

As there was a trace of oxygen in our experiments, we tested the influence of the presence of oxygen gas on the aggregation of nanoparticles. In a separate experiment, an aliquot of 100$\times$ diluted NPs (10 nM) in deaerated water containing 10 mM hydrazine was freeze dried in absence of air (inside a 'glovebag' filled with Ar gas) on a piece of silicon wafer. As shown in Figure 4.9, many more and larger aggregates are visible on the silicon when were hydrazine was injected when compared to samples with nanoparticles but without hydrazine (though isolated aggregates are observable in the absence of hydrogen (see Figure 4.9C)). This result indicates that also outside the electrochemical cell, in the strict absence of oxygen, the presence of hydrazine will induce the aggregation of Pt NPs.

Finally, the addition of 10 mM of hydrazine to a five-times diluted solution (~300 nM) of Pt NPs resulted in complete precipitation of the NPs overnight.

4.4 Discussion

In agreement with the pioneering experiments of Bard et al., injection of Pt nanoparticles into an electrochemical cell that contains hydrazine in phosphate buffer and a Au UME, discrete current steps are observed that indicate the arrival of nanoparticles that stick to the electrode surface. Although we observe a lower landing frequency than expected from theory and prior experiment, the amplitude of the current steps is in agreement with the previous experiments and with the expectations based on the model that the current peaks correspond to the diffusion-limited oxidation of hydrazine on the freshly landed Pt nanoparticle.

The reduced landing frequency could be related to a reduced effective nanoparticle concentration, related to the hydrazine-induced aggregation of particles in solution. This reasoning is corroborated by the outcome of additional experiments performed on the system. Using SEM, we observe aggregates on the surface of electrodes after Pt NP landing experiments in presence of hydrazine. We believe these aggregates are Pt because blank voltammetry on the electrode after landing experiments shows

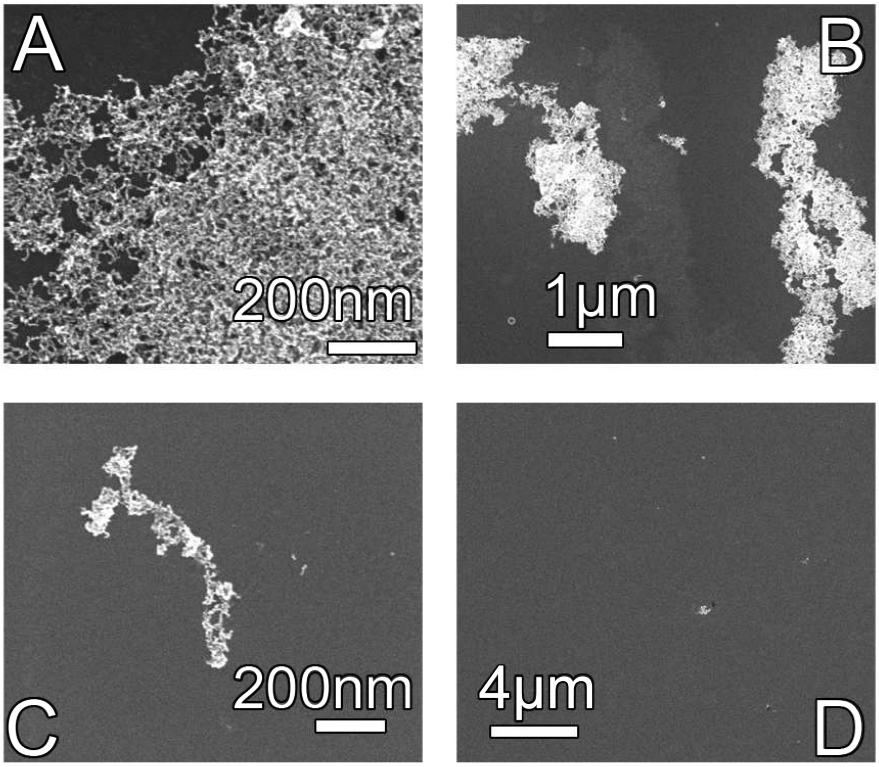

Figure 4.9: SEM images of nanoparticle aggregation observed after freeze drying 200 µL of 100x diluted Pt NPs in presence (A and B) and absence (C and D) of 10 mM hydrazine on a piece of Si in the absence of air.

Pt features. Moreover, very large aggregates are observed after drying in particles in the presence of hydrazine. The applied potential during landing experiments does not appear to influence the level of aggregation, suggesting that aggregation does not occur due to electrostatic interactions with the electrode. Instead, landing measurements in the absence of hydrazine, which are not observable electrochemically, lead to no aggregates visible under SEM. The electrode after this procedure does show a marked change in its voltammogram as visible in Figure 4.6A, indicative of Pt presence. This suggests that Pt is present in a form that we do not detect with the SEM, of which individual NPs would be the most likely candidate.

While hydrazine and hydrogen both appear to aggregate Pt NPs, the mechanism that governs this behavior is not completely clear. As oxygen gas does not play a role

in the mechanism of aggregation, this would exclude an 'electroless' reaction (i.e. oxidation of hydrazine, reduction of oxygen) on the surface of the Pt NPs as the cause of aggregation. We have examined the equilibrium potential of a flame-annealed platinum electrode in a phosphate buffer solution in the presence and absence of the reactants that surround the Pt NPs during landing experiments. As is known,[42] when Pt is in an electrolyte containing oxygen gas, it will maintain a potential of 0.9 V vs RHE, or the onset potential of the oxygen reduction reaction on Pt. If the oxygen is removed, the potential will eventually reach a value close to 0.1 V vs RHE. When hydrazine is injected to this solution the potential shifts negative to 0 V and after again adding oxygen to the system this potential is raised slightly to about 0.1 V. The presence of citrate does not influence these potentials. That is, when repeating the experiment in the presence of citrate, the potentials remain close to those found on a bare Pt electrode. This suggests that the interactions between Pt and citrate are rather weak. It has been reported previously,[43] that the tendency of dissolved citrate to replace hydrogen in the H_{UPD} of the Pt blank cyclic voltammogram is low, which means that hydrogen atoms adsorb stronger on Pt than citrate. Also, Lipkowski et al.[44] have performed chronocoulometric measurements on a Au (111) surface in presence of citrate. From the change in the surface charge they concluded that the citrate ions attach to the surface in deprotonated form, forming an overlayer on the surface that is similar to that of adsorbed sulfate from 0.2 V vs RHE.

Alternatively, hydrazine or hydrogen may displace the citrate ions, by having a stronger affinity to attach to the surface atoms. It has been noted before that Pt particles aggregate when hydrogen gas is added,[45] while it was found in early SERS studies that pyridine acts to aggregate Au particles.[46] It was suggested by Weitz et al.[47] that pyridine attaches stronger to the surface than the citrate ions do and displaces the citrate upon adsorption, as the citrate SERS signal is diminished in intensity with the onset of the signal for adsorbed pyridine. Moreover, amine groups attach to Au surface,[48, 49] similarly to the Au-thiol interaction (although the interaction is weaker). These reports in the literature focus mainly on Au, which is the more inert noble metal, but hydrazine must interact with a Pt surface in some way. Since only nitrogen gas has been found as the oxidation product of hydrazine on Pt,[33] hydrazine must adsorb or interact in undissociated form prior to oxidation on the platinum surface, and this interaction dislodges citrate from the Pt surface. In general, it seems that we must consider that the citrate shell around Pt nanoparticles is rather weakly adsorbed. We believe that a similar mechanism, as reported in our recent report,[50] utilizing H_2O_2 to remove the PVP capping-agent from Pt NPs may be operable between N_2H_4 and

Pt NPs.

The shape of the Pt NP aggregates suggests diffusion-limited aggregation, rather than reaction-limited aggregation.[51] The observed anisotropy means that nanoparticles attach with high probability when they meet. Hydrazine is a factor of ten million more concentrated in our electrolyte than the Pt NPs, so that the hydrazine-platinum interaction is not expected to be the rate limiting factor. Regarding the linear shape of the aggregates, it has been suggested by Turkevich[52] that when nanoparticle doublets are formed due to aggregation, the combined repulsive field is weakest at the ends, so that additional particles would feel lowest repulsion in a linear arrangement. This was based on the finding of two-dimensional Au NP chains formed under conditions of 'slow coagulation', namely diluted nanoparticle colloids in various concentrations of sodium perchlorate. These might be considered comparable to the conditions in our system.

If Pt NPs aggregate in the presence of hydrazine, the landing events detected in the chronoamperometry are due to the landing of both single NPs, but now at a (much) lower concentration than nominal, as well as of (large) aggregates of Pt NPs. This would explain both the lower landing frequency of the single NPs (as compared to theory) and the tailing observed in the size distributions. We cannot distinguish whether the current peaks are due to the landing of Pt NPs on the Au UME rather than on the Pt NP aggregate, as we cannot see the individual NPs in our SEM. Moreover, we do not know (how to recognize) the chronoamperometric response of the large aggregates that are observed in the SEM. Nevertheless, on the basis of our results, we must conclude that under present experimental circumstances, this experiment does not appear suited for the controlled attachment of a well-defined number of single nanoparticles on an ultramicroelectrode.

4.5 Conclusions

A recently developed method for the detection of nanoparticles[15–27] was investigated as a potential method to immobilize individual particles for the electrochemical study of their catalytic properties. This method consists of analyzing the current steps that can be measured at a Au UME when a colloid of Pt NPs is injected into an electrolyte containing hydrazine, because Pt is a better catalyst for N_2H_4 than Au. We have measured current steps attributed to the electrocatalytically amplified landing of Pt NPs on a lithographically fabricated Au UME and the modal step size is comparable to theory and prior measurements. [16] In our measurements, the landing frequency was

lower than values reported in the literature and those predicted from theory. Moreover, the current step distribution showed a long tail of large current steps. Both these findings suggest the presence of aggregated particles in solution, which lower the landing frequency by reducing the effective NP concentration and provide a higher current step upon reaching the electrode. Cyclic voltammetry measured after the landings showed a signal characteristic for Pt presence, while electron microscopy revealed that the NPs were in fact present as aggregates, after landings were performed in the presence of hydrazine or hydrogen gas. Only when particles were landed on the surface in absence of such reducing agents did we find no aggregates on the electrode surface, while CV still indicated the presence of Pt, suggesting the presence of individual particles.

We have also found that the absence of dissolved oxygen gas does not prevent the aggregation. Therefore we discard the idea that the aggregation is due to a change in the particles' surface potential when performing a catalytic oxidation in solution enabled by oxygen reduction. We tentatively ascribe the mechanism of aggregation to the interaction of these reducing agents with the NP surface that is possible owing to the weak interaction between citrate and Pt.

The finding, that landing nanoparticles in the presence of hydrazine yields NP aggregates on the surface, means that this particular method is currently not suited for the preparation of individually immobilized particles to facilitate catalysis studies at individual nanoparticles.

Bibliography

[1] Raimondi, F.; Scherer, G. G.; Kötz, R.; Wokaun, A. *Angewandte Chemie International Edition* 2005, *44*(15), 2190–2209.

[2] Kreibig, U.; Vollmer, M. *Optical Properties of Metal Clusters;* Springer, Heidelberg: Berlin, 1995.

[3] Zijlstra, P.; Orrit, M. *Rep. Prog. Phys.* 2011, *74*(10), 106401.

[4] Maillard, F.; Eikerling, M.; Cherstiouk, O. V.; Schreier, S.; Savinova, E.; Stimming, U. *Faraday Discuss.* 2004, *125*, 357–377.

[5] Koper, M. T. M. *Nanoscale* 2011, *3*(5), 2054–2073.

[6] Van Santen, R. A. *Acc. Chem. Res.* 2008, *42*(1), 57–66.

[7] Somorjai, G.; Park, J. *Top. Catal.* 2008, *49*(3), 126–135.

[8] Haruta, M. *Catal. Today* 1997, *36*(1), 153–166.

[9] Buurmans, I. L. C.; Ruiz-MartÃnez, J.; Knowles, W. V.; van der Beek, D.; Bergwerff, J. A.; Vogt, E. T. C.; Weckhuysen, B. M. *Nat Chem* 2011, *3*(11), 862–867.

[10] Claessen, V. I.; Engelkamp, H.; Christianen, P. C.; Maan, J. C.; Nolte, R. J.; Blank, K.; Rowan, A. E. *Annu. Rev. Anal. Chem.* 2010, *3*(1), 319–340.

[11] Chen, S.; Kucernak, A. *J. Phys. Chem. B* 2004, *108*(10), 3262–3276.

[12] Chen, S.; Kucernak, A. *J. Phys. Chem. B* 2004, *108*(37), 13984–13994.

[13] Lai, S. C. S.; Dudin, P. V.; Macpherson, J. V.; Unwin, P. R. *J. Am. Chem. Soc.* 2011, *133*(28), 10744–10747.

[14] Hoeben, F. J. M.; Meijer, F. S.; Dekker, C.; Albracht, S. P. J.; Heering, H. A.; Lemay, S. G. *ACS Nano* 2008, *2*(12), 2497–2504.

[15] Xiao, X.; Bard, A. J. *J. Am. Chem. Soc.* 2007, *129*(31), 9610.

[16] Xiao, X.; Fan, F.-R. F.; Zhou, J.; Bard, A. J. *J. Am. Chem. Soc.* 2008, *130*(49), 16669–16677.

[17] Xiao, X.; Pan, S.; Jang, J. S.; Fan, F.-R. F.; Bard, A. J. *J. Phys. Chem. C* 2009, *113*(33), 14978–14982.

[18] Kwon, S. J.; Zhou, H.; Fan, F.-R. F.; Vorobyev, V.; Zhang, B.; Bard, A. J. *Phys. Chem. Chem. Phys.* 2011, *13*(12), 5394–5402.

[19] Kwon, S. J.; Fan, F.-R. F.; Bard, A. J. *J. Am. Chem. Soc.* 2010, *132*(38), 13165–13167.

[20] Zhou, H.; Fan, F.-R. F.; Bard, A. J. *J. Phys. Chem. Lett.* 2010, *1*(18), 2671–2674.

[21] Zhou, Y.-G.; Rees, N. V.; Compton, R. G. *Angewandte Chemie International Edition* 2011, *50*(18), 4219–4221.

[22] Zhou, Y.-G.; Rees, N. V.; Compton, R. G. *Chem. Phys. Lett.* 2011, *511*(4-6), 183–186.

[23] Zhou, Y.-G.; Rees, N. V.; Compton, R. G. *ChemPhysChem* 2011, *12*(11), 2085–2087.

[24] Zhou, Y.-G.; Rees, N. V.; Pillay, J.; Tshikhudo, R.; Vilakazi, S.; Compton, R. G. *Chem. Commun.* 2012, *48*(2), 224–226.

[25] Zhou, Y.-G.; Rees, N. V.; Compton, R. G. *Chem. Commun.* 2012, *48*(19), 2510–2512.

[26] Zhou, Y.-G.; Rees, N. V.; Compton, R. G. *Chem. Phys. Lett.* 2011, *514*(4-6), 291–293.

[27] Rees, N. V.; Zhou, Y.-G.; Compton, R. G. *ChemPhysChem* 2011, *12*(9), 1645–1647.

[28] Lin, C.-S.; Khan, M. R.; Lin, S. D. *J. Colloid Interface Sci.* 2005, *287*(1), 366–369.

[29] Grobelny, J.; DelRio, F. W.; Pradeep, N.; Kim, D.-I.; Hackley, V. A.; Cook, R. F. In *Methods in Molecular Biology*; Walker, J., Ed., Vol. 697 of *Methods in Molecular Biology;* Springer, Heidelberg, 2009; pages 71–82.

[30] Horcas, I.; Fernandez, R.; Gomez-Rodriguez, J.; Colchero, J.; Gomez-Herrero, J.; Baro, A. *Rev. Sci. Instrum.* 2007, *78*, 013705.

[31] Jentys, A. *Phys. Chem. Chem. Phys.* 1999, *1*(17), 4059–4063.

[32] Patterson, A. L. *Phys. Rev.* 1939, *56*(10), 978–982.

[33] Rosca, V.; Koper, M. T. M. *Electrochim. Acta* 2008, *53*(16), 5199–5205.

[34] Aldous, L.; Compton, R. G. *Phys. Chem. Chem. Phys.* 2011, *13*(12), 5279–5287.

[35] Dudin, P. V.; Unwin, P. R.; Macpherson, J. V. *Phys. Chem. Chem. Phys.* 2011, *13*(38), 17146–17152.

[36] Alvarez-Ruiz, B.; Gomez, R.; Orts, J. M.; Feliu, J. M. *J. Electrochem. Soc.* 2002, *149*(3), D35–D45.

[37] Bard, A. J.; Faulkner, L. R. *Electrochemical Methods, Fundamentals and Applications;* John Wiley & Sons: New York, 2 ed., 2001.

[38] Kleijn, S. E. F.; Yanson, A. I.; Koper, M. T. M. *J. Electroanal. Chem.* 2012, *666*(0), 19–24.

[39] Zare, H. R.; Nasirizadeh, N. *Electroanalysis* 2006, *18*(5), 507–512.

[40] Ardakani, M. M.; Karimi, M.; M.M., Z.; Mirdehghan, S. *Int. J. Electrochem. Sci.* 2008, *3*, 246 – 258.

[41] Angerstein-Kozlowska, H.; Conway, B. E.; Barnett, B.; Mozota, J. *J. Electroanal. Chem. Interfac. Electrochem.* 1979, *100*, 417–446.

[42] Wroblowa, H.; Rao, M. L. B.; Damjanovic, A.; Bockris, J. O. *J. Electroanal. Chem. Interfac. Electrochem.* 1967, *15*(0), 139–150.

[43] González-Peña, O. I.; Chapman, T. W.; Vong, Y. M.; Antaño López, R. *Electrochim. Acta* 2008, *53*(17), 5549–5554.

[44] Kunze, J.; Burgess, I.; Nichols, R.; Buess-Herman, C.; Lipkowski, J. *J. Electroanal. Chem.* 2007, *599*(2), 147–159.

[45] Furlong, D. N.; Launikonis, A.; Sasse, W. H. F.; Sanders, J. V. *Journal of the Chemical Society, Faraday Transactions 1: Physical Chemistry in Condensed Phases* 1984, *80*(3), 571–588.

[46] Creighton, J. A.; Blatchford, C. G.; Albrecht, M. G. *Journal of the Chemical Society, Faraday Transactions 2: Molecular and Chemical Physics* 1979, *75*, 790–798.

[47] Weitz, D. A.; Lin, M. Y.; Sandroff, C. J. *Surf. Sci.* 1985, *158*, 147–164.

[48] Venkataraman, L.; Klare, J. E.; Tam, I. W.; Nuckolls, C.; Hybertsen, M. S.; Steigerwald, M. L. *Nano Lett.* 2006, *6*(3), 458–462.

[49] Leff, D. V.; Brandt, L.; Heath, J. R. *Langmuir* 1996, *12*(20), 4723–4730.

[50] Monzó, J.; Koper, M. T. M.; Rodriguez, P. *ChemPhysChem* 2012, *13*(3), 709–715.

[51] Lin, M. Y.; Lindsay, H. M.; Weitz, D. A.; Ball, R. C.; Klein, R.; Meakin, P. *Nature* 1989, *339*(6223), 360–362.

[52] Enüstün, B. V.; Turkevich, J. *J. Am. Chem. Soc.* 1963, *85*(21), 3317–3328.